Pure Appl. Geophys.

https://doi.org/10.1007/s00024-020-02526-9

Pure and Applied Geophysics

Connection of Seismic Noise Properties in Japan and California with Irregularity of Earth's Rotation

Alexey Lyubushin[1]

Abstract—The problem of the relationship of the properties of seismic noise with the irregular rotation of the Earth is considered. We study the median daily values of the multifractal singularity spectrum support width, the generalized Hurst exponent, and the seismic noise wavelet-based entropy on the networks of broadband seismic stations in Japan and California for the time interval 1997–2019. The first principal components of the noise properties in a half year moving time window are calculated. The coherence spectra are estimated both between the principal noise components in two regions and each principal component with a time series of the length of day (LOD). It has been shown that an increase in the power of high-frequency pulsations of LOD (for periods less than 6 days) is accompanied by a decrease in the coherence between the properties of seismic noise in Japan and California. The degree of synchronization of the response of changes in the properties of seismic noise in Japan and California to the irregularity of Earth's rotation in a "long" moving time window of 5 years is estimated. For this purpose, the correlation coefficient and the "secondary" coherence spectrum between synchronous variations of the "primary" coherence spectra between the LOD and each of the main noise components obtained in the "short" half-year window, as well as their mutual correlation function, were calculated.

Keywords: Seismic noise, length of day, multifractals, entropy, principal component analysis, correlation, coherence, vector autoregression.

1. Introduction

The property of the uneven rotation of the Earth has traditionally attracted the attention of geophysicists. The explanation of this effect is mainly based on estimates of the influence of processes in the atmosphere (Zotov et al. 2016). At the same time, many researchers have repeatedly pointed out the relationship between the uneven rotation of the Earth and seismicity (Shanker et al. 2001; Levin et al. 2017). In this case, the main attention was paid to the possible trigger mechanism of the effect of variations in the planet rotation speed on the seismic process (Bendick and Bilham 2017). Note that with this interpretation, a logical question arises about the impact of atmospheric processes (including climate variations) through the irregular rotation of the Earth on the seismic process.

This article discusses the relationship between seismic noise in Japan and California with the LOD (length of day) parameter, which presents a sequence of day length values and the characteristic of the irregular rotation of the Earth. The relationship between the properties of global seismic noise and the LOD time series was previously investigated in Lyubushin (2020), where it was shown that mid-2003 is a break point in the trends and correlations of global seismic noise properties. After 2003, trends acquire the character inherent in areas with increasing seismic hazard. Note that after the Sumatran mega-earthquake of December 26, 2004, M = 9, there was a sharp increase in the number of strongest earthquakes around the world.

This article is a logical continuation of this study, but from the global level we are going down to the regional one and the main attention is paid to the noise properties in two active regions separated by the Pacific Ocean—Japan and California. The presence of networks of broadband stations, the data of which is freely available over the Internet for the period from the beginning of 1997 to the current time, makes it possible to study in detail both the noise properties in connection to irregularity of Earth's rotation within these regions and the degree of correlation between them.

[1] Institute of Physics of the Earth, Russian Academy of Sciences, Moscow, Russia. E-mail: lyubushin@yandex.ru

Published online: 02 June 2020

Seismic noise is considered as a manifestation of the inner life of the planet and as an important "communication channel" that allows us to study processes in the lithosphere, including those that anticipate strong earthquakes (Lyubushin 2012, 2013, 2018a, b). Assuming that earthquakes are the main source of energy for the Earth's global seismic background, estimates show that in order to maintain the observed amount of energy, at least one magnitude 6 earthquake should occur daily. However, the total contribution of all weak earthquakes, according to the Gutenberg–Richter law, is one to two orders of magnitude lower than the real energy of constant seismic noise. As a result of such estimates, it was concluded that the movement of cyclones in the atmosphere, the influence of waves on the shelf and coast, as well as climate change, make the main contribution to the energy of low-frequency seismic noise (Ardhuin et al. 2011; Aster et al. 2008; Friedrich et al. 1998; Grevemeyer et al. 2000; Kobayashi and Nishida 1998; Rhie and Romanowicz 2004, 2006; Tanimoto 2001, 2005).

Considering the earth's crust as a medium of seismic wave propagation from sources external to it (ocean and atmosphere), we assume that the processes inside the earth's crust are reflected in changes in the statistical properties of seismic noise and the study of these properties allows us to determine the structural features of the earth's crust (Berger et al. 2004; Fukao et al. 2010; Koper et al. 2008, 2010; Nishida et al. 2008, 2009; Stehly et al. 2006). In particular, changes in noise properties can be a source of information about changes in the earth's crust that accompany the seismic process (Lyubushin 2010, 2014a, b, 2015).

2. Data

Figure 1 shows the locations of the stations of two broadband seismic networks in Japan and California, the data of which are used in this study.

The first data set was taken from the F-net network in the Japanese Islands (84 stations), which can be downloaded from the address: https://www.fnet.bosai.go.jp/faq/?LANG=en. The second data set was taken from the union of three regional networks in California, the data of which are presented at the addresses: https://ds.iris.edu/mda/AZ; https://ds.iris.edu/mda/BK; https://ds.iris.edu/mda/CI and is supported by 141 stations. For the analysis, a time interval of 23 years was selected: 1997–2019. Figure 1 shows the locations of seismic station networks in Japan and California. For analysis in California, those stations were selected that have broadband sensors and LHZ data, that is, vertical oscillations with a sampling frequency of 1 Hz. The data of vertical components with a sampling frequency of 1 Hz were downloaded, which were then reduced to a time step of 1 min by calculating the average values in successive time intervals of 60 values in length.

3. Statistics for Seismic Noise Analysis

3.1. Minimum Normalized Entropy of Wavelet Coefficients En

Let $x(t)$ be a finite sample of some random signal, $t = 1, \ldots, N$ be an index numbering consecutive samples (discrete time). We define the normalized entropy by the formula:

$$En = -\sum_{k=1}^{N} p_k \cdot \log(p_k)/\log(N), \quad p_k = c_k^2 / \sum_{j=1}^{N} c_j^2, \quad 0 \le En \le 1 \tag{1}$$

Here c_k, $k = 1, N$ are the coefficients of the orthogonal wavelet decomposition with some basis. The following 17 orthogonal Daubechies wavelets were used: 10 ordinary bases with minimal support with the number of vanishing moments from 1 to 10 and 7 so-called Daubechies symlets (Mallat 1999), with the number of vanishing moments from 4 to 10. For each of the bases, the normalized entropy of the square distribution was calculated coefficients (1) and found a basis that provides a minimum value of (1). Note that due to the orthogonality of the wavelet transform, the sum of the squared coefficients is equal to the variance (energy) of the signal $x(t)$. Thus, quantity (1) calculates the entropy of the distribution of energy of oscillations at various frequency and time scales. Entropy (1) by construction has much in common with multiscale entropy (Costa et al.

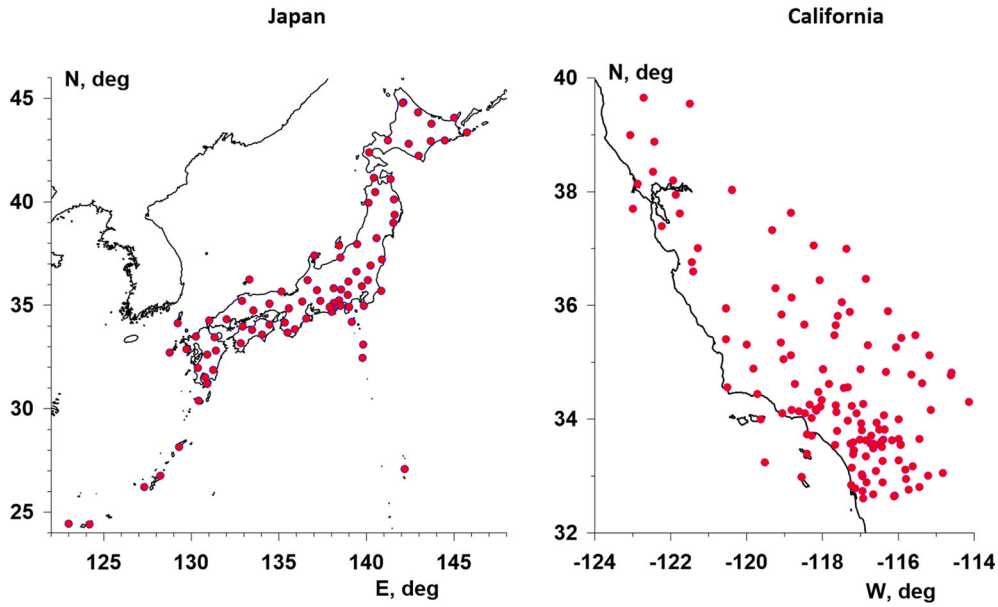

Figure 1
On the left are the positions of 84 seismic stations in Japan, on the right are the positions of 141 stations in California

2003, 2005). It should also point out the related construction of entropy based on the use of the natural time approach (Sarlis et al. 2018; Varotsos et al. 2011).

3.2. Multifractal Parameters $\Delta\alpha$, α^*

Let us define the measure of variability $\mu_X(t,\delta)$ of signal $x(t)$ on the time interval $[t, t+\delta]$ as the difference between maximum and minimum values $\mu_x(t,\delta) = \max_{t\le u\le t+\delta} x(u) - \min_{t\le u\le t+\delta} x(u)$ and calculate the mean value of its power degree q: $M(\delta,q) = M[(\mu_x(t,\delta))^q]$. A random signal is scale-invariant (Taqqu 1988) if $M(\delta,q)\sim \delta^{\rho(q)}$ when $\delta\to 0$, that is, the following limit exists:

$$\rho(q) = \lim_{\delta\to 0}(\ln M(\delta,q)/\ln\delta) \tag{2}$$

If $\rho(q)$ is a linear function $\rho(q) = Hq$, where $H = const$, $0<H<1$, the process is called mono-fractal. In the case where $\rho(q)$ is a nonlinear concave function of q, the signal is called multifractal. To estimate the value of $\rho(q)$ using a finite sample $x(t)$, $t = 0,1,\ldots,N-1$ we used the method, which is based on the approach of detrended fluctuation analysis (DFA) (Kantelhardt et al. 2002). Let us split the entire time series into non-overlapping intervals of length s:

$$I_k^{(s)} = \{t:\ 1+(k-1)s\le t\le ks,\quad k = 1,\ldots,[N/s]\} \tag{3}$$

and let

$$y_k^{(s)}(t) = x((k-1)s+t),\quad t = 1,\ldots,s \tag{4}$$

be a part of the signal $x(t)$, corresponding to interval $I_k^{(s)}$. Let $p_k^{(s,m)}(t)$ be a polynomial of the order m, best fitted to the signal $y_k^{(s)}(t)$ by least squares method. Let us consider the deflections from the local trend:

$$\Delta y_k^{(s,m)}(t) = y_k^{(s)}(t) - p_k^{(s,m)}(t),\quad t = 1,\ldots,s \tag{5}$$

and calculate the values

$$Z^{(m)}(q,s) = \left(\sum_{k=1}^{[N/s]}\left(\max_{1\le t\le s}\Delta y_k^{(s,m)}(t) - \min_{1\le t\le s}\Delta y_k^{(s,m)}(t)\right)^q\right/ [N/s]\Big)^{1/q} \tag{6}$$

that can be regarded as the estimate of $(M(\delta_s,q))^{1/q}$. Let us define the function $h(q)$ as a coefficient of linear regression between $\ln(Z^{(m)}(q,s))$ and $\ln(s)$: $Z^{(m)}(q,s)\sim s^{h(q)}$ fitted for scales range

$s_{\min} \le s \le s_{\max}$. It is evident that $\rho(q) = qh(q)$ and, for a mono-fractal signal, $h(q) = H = const$. The multifractal singularity spectrum $F(\alpha)$ is equal to the fractal dimensionality of the set of time moments t for which the Hölder–Lipschitz exponent is equal to α i.e. for which $|x(t+\delta) - x(t)| \sim |\delta|^{\alpha}, \quad \delta \to 0$ (Feder 1988). The singularity spectrum can be estimated using the standard multifractal formalism, which consists in calculating the Gibbs sum:

$$W(q,s) = \sum_{k=1}^{[N/s]} \left(\max_{1 \le t \le s} \Delta y_k^{(s,m)}(t) - \min_{1 \le t \le s} \Delta y_k^{(s,m)}(t) \right)^q \tag{7}$$

and in estimating the mass exponent $\tau(q)$ from the condition $W(q,s) \sim s^{\tau(q)}$. From Eq. (6) it follows that $\tau(q) = \rho(q) - 1 = qh(q) - 1$. In the next step, the spectrum $F(\alpha)$ is calculated with the Legendre transform:

$$F(\alpha) = \max \{ \min_q (\alpha q - \tau(q)),\ 0 \} \tag{8}$$

If the singularity spectrum $F(\alpha)$ is estimated in a moving window, its evolution can give useful information on the variations in the structure of the "chaotic" pulsations of the series. In particular, the position and width of the support of the spectrum $F(\alpha)$, i.e., the values $\alpha_{\min}, \ \alpha_{\max}, \quad \Delta\alpha = \alpha_{\max} - \alpha_{\min}$, and α^*, such that $F(\alpha^*) = \max_{\alpha} F(\alpha)$, are characteristics of the noisy signal. The value α^* can be called a generalized Hurst exponent and it gives the most typical value of Lipschitz–Holder exponent. Parameter $\Delta\alpha$, singularity spectrum support width, could be regarded as a measure of variety of stochastic behavior. In the case of a mono-fractal signal, the quantity $\Delta\alpha$ should vanish and $\alpha^* = H$. Usually $F(\alpha^*) = 1$, but there exist time windows for which $F(\alpha^*) < 1$.

Multifractal characteristics are widely used to analyze geophysical time series and search for precursors of strong seismic events, for example (Varotsos et al. 2003a, 2003b; Ramirez-Rojas et al. 2004; Currenti et al. 2005; Telesca and Lovallo 2011). Statistics $\Delta\alpha$, α^* and En were used in Lyubushin (2012, 2013, 2014a, b, 2015, 2018a, b) to study the synchronization properties of the global seismic noise field and the prognostic properties of seismic noise in the Japanese islands.

Figure 2 shows graphs of median values $\Delta\alpha$, α^* and En calculated each day for all operable stations of seismic networks in Japan and California. These statistics were calculated within adjacent time windows of the length 1440 samples with time step 1 min. Entropy En was computed after removing trends in each time window by polynomial of 8th order. Multifractal parameters $\Delta\alpha$, α^* were calculated after removing scale dependent local trends using Eq. (5) by polynomials of 8th order ($m = 8$) as well. Removing trends is necessary to get rid of deterministic tidal and temperature influences for investigating random seismic noise properties.

It should be noticed that using of multifractal parameters and especially singularity spectrum support width $\Delta\alpha$ has a rather long history in investigation of nonlinear systems behavior. Particularly the "loss of multifractality" i.e. decreasing of singularity spectrum support width, is a well-known effect before the abrupt change of different system properties. Mainly this effect was investigated in biological and medicine systems (Ivanov et al. 1999; Humeaua et al. 2008; Dutta et al. 2013), but in Pavlov and Anishchenko (2007) it was shown that it has a rather universal character and is observed in physical systems as well. The analogy between effect of singularity spectrum support narrowing of seismic noise waveforms and the loss of multifractality in the behavior of other nonlinear systems gave an impulse to the author to make a hypothesis about approaching Japanese island to seismic catastrophe (Lyubushin 2008). Entropy En of seismic noise possesses similar properties as $\Delta\alpha$ but with opposite sign—it increases before strong earthquakes (Lyubushin 2012, 2018a). Thus, multifractal and entropy properties of seismic noise are rather sensitive to changes in the Earth's crust. That was the reason for choosing vector $(En, \Delta\alpha, \alpha^*)$ as some kind of phase space of seismically active regions.

4. *Principal Components of Seismic Noise Properties*

There is a need to aggregate time series $(En, \Delta\alpha, \alpha^*)$ into one time series, which carries the most common properties from the initial set of seismic noise property parameters. We used here a

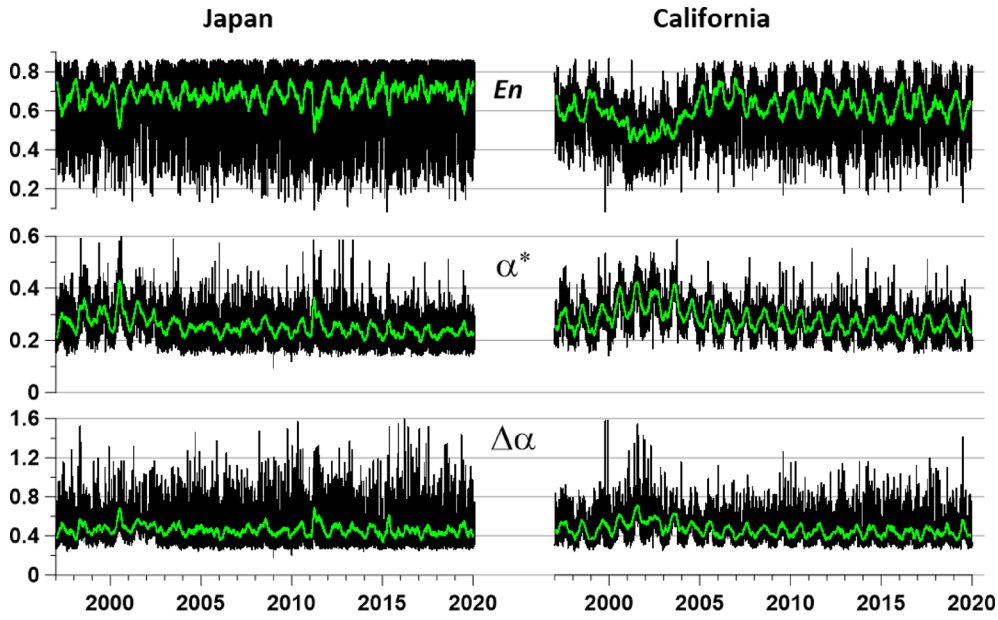

Figure 2
On the left there are graphs of daily median parameter values $(En, \Delta\alpha, \alpha^*)$ in Japan, on the right are graphs of the same parameters for California. Green lines represent moving averages in a 57-day window

modification of the popular principal component method (Jolliffe 1986) proposed in Lyubushin (2018a). Let $P(t) = (P_1(t), \ldots, P_m(t))^T$, $t = 0, 1, \ldots$—several time series of total dimension m. In our case $m = 3$. Let L be the number of samples within the time window, which moves from left to right with a minimum mutual shift of 1, which we will call the "adaptation window". Let s be the reference number corresponding to the right-hand end of the moving time window. This means that the time window contains samples with time indices that obey the condition $s - L + 1 \le t \le s$. We calculate the correlation matrix $\Phi(s)$ of the size $m \times m$ in each time window after normalizing the components of the time series:

$$\Phi(s) = \left(\varphi_{ab}^{(s)}\right), \quad \varphi_{ab}^{(s)} = \sum_{t=s-L+1}^{s} q_a^{(s)}(t) q_b^{(s)}(t)/L, \quad a, b = 1, \ldots, m \tag{9}$$

where

$$q_a^{(s)}(t) = (P_a(t) - \overline{P}_a^{(s)})/\sigma_a^{(s)}, \quad \overline{P}_a^{(s)} = \sum_{t=s-L+1}^{s} P_a(t)/L,$$
$$\left(\sigma_a^{(s)}\right)^2 = \sum_{t=s-L+1}^{s} (P_a(t) - \overline{P}_a^{(s)})^2/(L-1), \quad a = 1, \ldots, m \tag{10}$$

First principal component $\psi^{(s)}(t)$ is calculated according to the formula:

$$\psi^{(s)}(t) = \sum_{\alpha=1}^{m} \theta_a^{(s)} \cdot q_a^{(s)}(t) \tag{11}$$

Here the m-dimensional vector $\theta^{(s)} = (\theta_1^{(s)}, \ldots, \theta_m^{(s)})^T$ is an eigenvector of the correlation matrix $\Phi(s)$ corresponding to its maximum eigenvalue. We define the scalar time series $\psi(t)$ of the adaptive first principal component in a sliding window with the length of L samples according to the formula:

$$\psi(t) = \begin{cases} \psi^{(L-1)}(t), & 0 \le t \le (L-1) \\ \psi^{(t)}(t), & t \ge L \end{cases} \tag{12}$$

The operations represented by formulas (4–6) are carried out independently in each time window by the

length of L samples. Thus, within the 1st adaptation time window, the time series $\psi(t)$ consists of values calculated according to Eq. (12). For all subsequent time windows $\psi(t)$ is taken as the value from Eq. (6) which corresponds to the right-hand end of the time window. It means that outside the 1st adaptation window $\psi(t)$ depends only on past values of $P(t)$.

Figure 3a shows the graphs of the time series of the length of day (LOD), which characterizes the irregular rotation of the Earth. Figure 3b shows a graph of the high-frequency LOD component with periods of no more than 6 days, which will play an important role in the subsequent data analysis. Figures 3c, d present the graphs of first principal components of 3 daily time series $(En, \Delta\alpha, \alpha^*)$ from each region (see Fig. 2) which are calculated according to Eq. (11) in a moving adaptation window of length $L = 182$ days (half year).

The data on the length of the day is taken from the International Earth rotation and Reference systems Service (IERS) database by the address: https://hpiers.obspm.fr/iers/eop/eopc04/eopc04.62-now.

5. Coherence Spectra by Vector Autoregression

Further data analysis is based on the calculation of the coherence spectra between two time series in a moving time window. For this purpose, we use a parametric model of vector autoregression. For a multidimensional time series $X(t)$ of dimension q, where t is the discrete time index, this model is given by the formula:

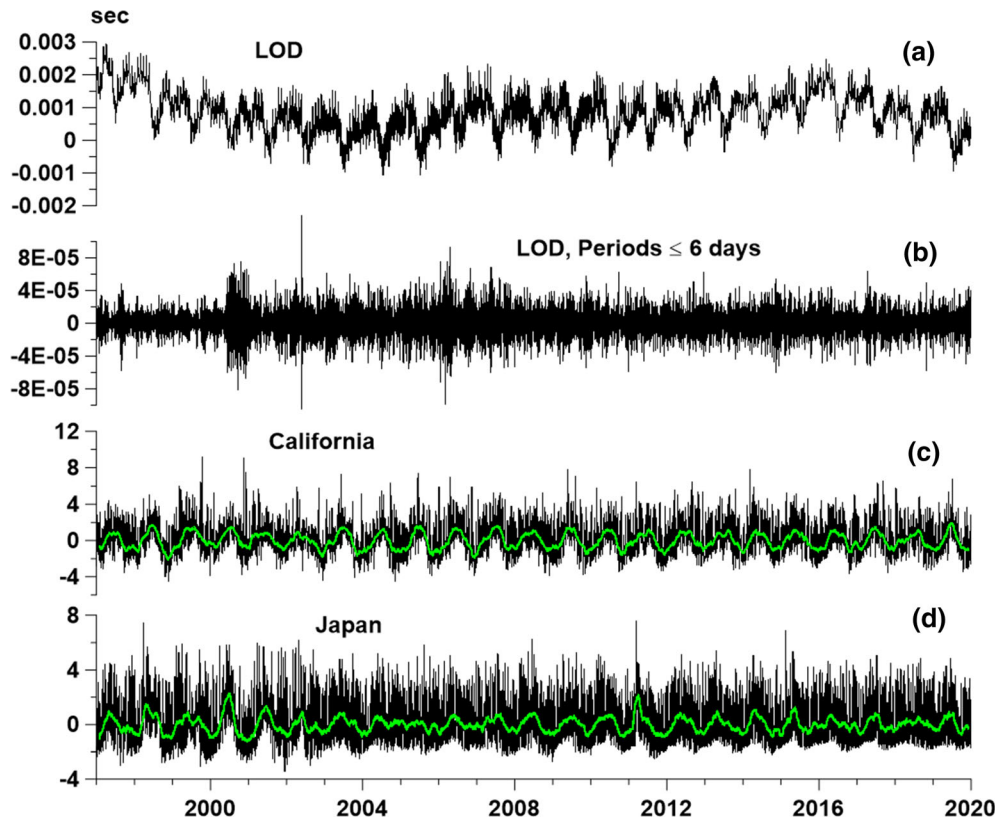

Figure 3
a Is a graph of the time series of the length of the day (LOD); **b**—a graph of high-frequency pulsations of LOD with periods of no more than 6 days; **c**, **d** are plots of the first principal components of the three median daily seismic noise properties in California and Japan, calculated in a moving time window of 182 days. Green lines represent moving averages in a 57-day window

$$X(t) + \sum_{k=1}^{p} B_k \cdot X(t-k) = \varepsilon(t) \qquad (13)$$

where p is the order of autoregression, B_k are the matrix of coefficients of autoregression of the size $q \times q$, $\varepsilon(t)$ is the residual signal with zero mean and covariance matrix $P = M\{\varepsilon(t)\varepsilon^T(t)\}$ of size $q \times q$. The matrices B_k and P are determined using the Durbin–Levinson procedure (Marple 1987), and the spectral matrix is calculated by the formula:

$$\begin{aligned} S_{XX}(\omega) &= \Phi^{-1}(\omega) \cdot P \cdot \Phi^{-H}(\omega), \Phi(\omega) \\ &= E + \sum_{k=1}^{p} B_k e^{-i\omega k} \end{aligned} \qquad (14)$$

where E is the unit size $q \times q$ matrix. If $q = 2$ then the quadratic coherence spectrum is calculated by the formula:

$$\gamma^2(\omega) = |S_{12}(\omega)|^2 \Big/ (S_{11}(\omega) \cdot S_{22}(\omega)) \qquad (15)$$

where $S_{11}(\omega)$ and $S_{22}(\omega)$ are the diagonal elements of matrix (14), that is, the parametric estimates of the power spectra of two signals, and $S_{12}(\omega)$ is their mutual cross-spectrum. The choice of a parametric model for calculating a two-dimensional spectral matrix is due to the fact that it has a better frequency resolution than conventional non-parametric methods for estimating the power spectrum and cross-spectra based on smoothing periodograms (Marple 1987).

Below we will apply estimates of the coherence spectra (15) in moving time windows. In Lyubushin (2018), two-dimensional vector autoregressive models were used to construct averaged coherence measures for multidimensional large-dimensional time series in a moving time window. As a result, the effects of global synchronization of the earth's tremor measured by the GPS network were discovered by processing daily time series from 1191 GPS stations around the world for the time interval 2006–2018.

6. Coherence Between Principal Components

As was shown in Lyubushin (2020), the minimum correlation between the properties of global seismic noise falls on the time interval 2001–2003, during which there is a sharp non-stationarity in high-frequency variations of the length of the day. Let us check how true this observation is at the regional level, in particular for the relationship between the properties of seismic noise in Japan and California. For this purpose, we calculate the coherence spectrum (9) between the first principal components of the seismic noise properties shown in Fig. 3. For calculations, we take a time window of 1826 days, which is usually 5 years. This window length takes into account that in a time interval of 5 years at least one year is a leap year and contains 366 days, except in rare cases when the 5-year period contains 2 leap years (in this case, 5 years are equal to 1827 days). We will take the displacement of the windows for 5 days and in each window we will evaluate the 10th-order two-dimensional autoregressive model (13). As a result, we obtain the time–frequency diagram presented in Fig. 4a. It gives map, where the sequence of squared coherence spectra, calculated according to Eq. (15) using two-dimensional autoregression model (13, 14), is presented in dependence on time value of

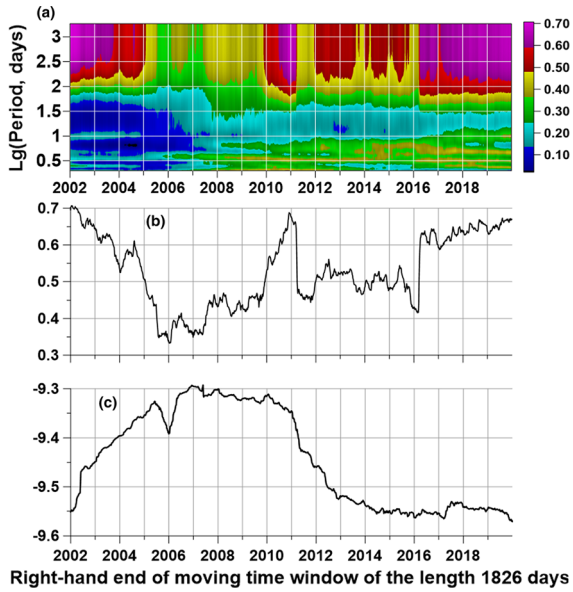

Figure 4

a A time–frequency diagram of the squared coherence spectrum between the first principal components of the properties of seismic noise in Japan and California in a window of 1826 days; **b** a graph of the maximum values of the squared coherence spectrum in a moving time window with a length of 1826 days between the first principal components of the properties of seismic noise; **c** the logarithm of the variance of LOD with periods of less than 6 days, calculated in a moving time window of 1826 days in length

right-hand end of moving time window of the length 1826 days (horizontal axis) and decimal logarithm of periods measured in days (vertical axis). The range of periods is from minimum value 2 days (Nyquist period) up to maximum 1826 days (the length of time window).

Figure 4b shows graphs of the maximum values of the coherence spectrum calculated for all frequency values in each time window. From these graphs it can be seen that the lows correspond to the marks of 2006–2007 of the right-hand end of the time window. Taking into account that the window is 5 years long, this means that the time interval for which the maximum coherence values are minimal is 2001–2007. To test the hypothesis proposed in Lyubushin (2020) that the reduced coherence or correlation of seismic noise properties can be caused by an increase in the power of high-frequency pulsations of the length of day, we calculate the variance of the LOD component with periods of no more than 6 days. The graph of the logarithm of this variance, also calculated in a moving time window of 5 years, is shown in Fig. 4c. Once again, we note that both the frequency–time diagram in Fig. 4a and the graphs in Fig. 4c, d are plotted depending on the position of the right-hand end of the moving time window with a length of 1826 days.

It is seen that the increase in the variance of high-frequency LOD component in Fig. 4c occurs simultaneously with the decrease in the maximum coherences in Fig. 4b. Further, after stabilization of the LOD variance values, coherence began to increase until the beginning of 2011, that is, until the Tohoku mega-earthquake in Japan on March 11, 2011. The fact that the coherence of the properties of seismic noise in Japan and California before the mega-earthquake in Japan was increased was noted in Lyubushin (2017). We also note that in Fig. 4c it can be seen that after the mega-earthquake in Japan, a rapid decline in the variance of high-frequency pulsations of LOD began. From a comparison of the graphs in Fig. 4b, c, we can conclude that the maximum coherence between the first principal components of seismic noise in Japan and California and the LOD variance in the time interval before March 11, 2011 are in antiphase—the correlation coefficient between them is equal to − 0.73.

7. *Primary Coherences Between Principal Components and LOD*

Now consider the relationship between the first principal components of seismic noise and LOD. For this, we calculate the sequence of coherence spectra between the increments of the first principal noise components in Japan and California and the LOD increments in a sliding time window of 182 days in length with a shift of 5 days. To calculate coherence, we again use the two-dimensional model of autoregression (13). The autoregression order is set equal to 5.

Figure 5a shows the time–frequency diagram of estimates of the coherence spectrum between the LOD and the first principal noise component in California. It can be seen from it that coherence is concentrated mainly in a narrow frequency band with periods from 8 to 19 days. The behavior of the coherence spectrum for Japan is of a similar nature and therefore the corresponding diagram is not presented.

For further analysis, we consider 2 time series of the maximum values of the squared coherence between the increments of the main components of the properties of seismic noise in California and Japan and LOD (see Fig. 3). Maxima are taken in each time window according to frequency values in diagrams of the type shown in Fig. 5a. Since coherence estimates were made in a moving time window of 182 days in length with a shift of 5 days, the time step for these time series is 5 days. The graphs of these time series and their histograms are presented in Fig. 5. From the histogram plots in Fig. 5b′, c′ it is seen that the values of the maximum coherence are mainly small and concentrated in the range 0.05–0.3. However, the distribution of coherence maxima is characterized by rather “heavy tails”, which correspond to significant bursts of values.

Further on, the sequence of maximum values of coherence with LOD will also be called “primary coherences”. The meaning of the term “primary coherence” is that we will further consider estimates of the coherence spectra between the time series presented in Fig. 5b, c, which we will call “secondary coherence”. An analysis of “secondary coherence”, that is, the coherence estimated in the

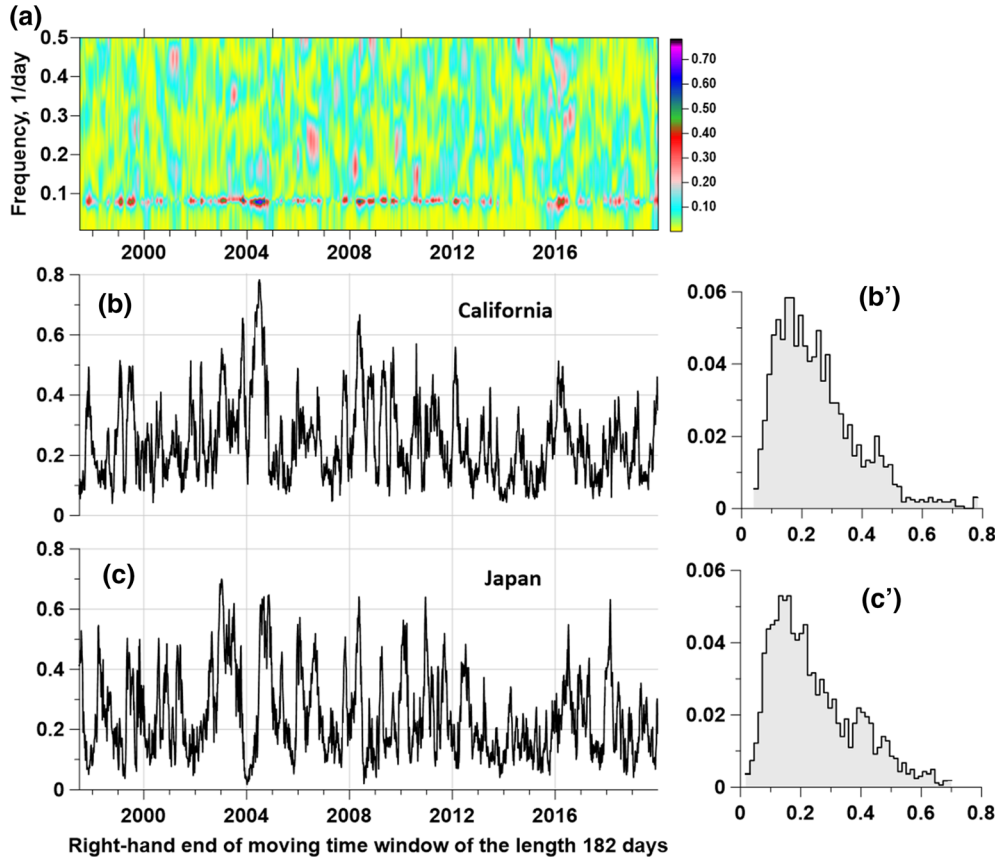

Figure 5
a A time–frequency diagram of the squared coherence spectrum between the LOD and the first principal component of the daily median values of the 3 properties of seismic noise in California in a moving time window of 182 days in length with a mutual shift of 5 days; **b**, **c** plots of the maxima of squared coherence spectra with respect to frequency values within each time window ("primary coherences"); **b′**, **c′** the corresponding histograms of the maximum values of the squared coherence

"long" window, from the values of the "primary" coherences previously calculated in the "short" time window, was proposed in Lyubushin (2019).

8. *Secondary Coherences*

We consider sequences of primary coherence values as a measure of the response of the effects of uneven rotation of the Earth to the properties of seismic noise in different regions. In connection with this interpretation, the question arises of how this effect is synchronous. Since the irregularity of the Earth's rotation is a global planetary process, a priori, a rather high correlation and coherence should be expected between the response of changes in the properties of seismic noise to LOD variations in two different regions, even despite their great remoteness from each other, like Japan and California.

Verification of this a priori assumption can be performed by calculating the values of the correlation coefficient between primary coherences, as well as estimating the spectral "secondary" coherence between them in a certain "long" time window. When choosing a "long" window, it should be borne in mind that the primary coherences were obtained by evaluating in "short" time windows 182 days long, taken with mutual shift of 5 days.

Thus, if we take adjacent L values of the primary coherences, then the dimension length of the "long"

time window will be equal to $N = 182 + (L - 1) \cdot 5$ days. When choosing $L = 330$ the value $N = 1827$ days. The number of days in 5 adjacent years is 1826 or 1827, taking into account the fact that in each interval of 5 years, either one or two years are leap years. Therefore, the choice $L = 330$ provides the time window length of 5 years with great accuracy, that is, the length of the time window that we used when plotting in Fig. 4.

Figure 6a shows a graph of the correlation coefficient between the primary coherences in a moving time window of 330 adjacent values (approximately 5 years) with a minimum shift of one value (5 days).

Figure 6b, c are related to the calculation of the modulus of the coherence spectrum between primary coherences also in a moving time window with a length of 330 values with an offset of 1 value. In contrast to the coherence estimates on Figs. 4 and 5 here it is shown the values of $\gamma(\omega)$ from formula (15). This difference is caused by the desire to compare the values of the correlation coefficient in Fig. 6a with the coherence modules, whereas $\gamma^2(\omega)$ corresponds to the frequency-dependent square of the correlation coefficient. For evaluation, a 2-dimensional model of vector autoregression of the 5th order was used.

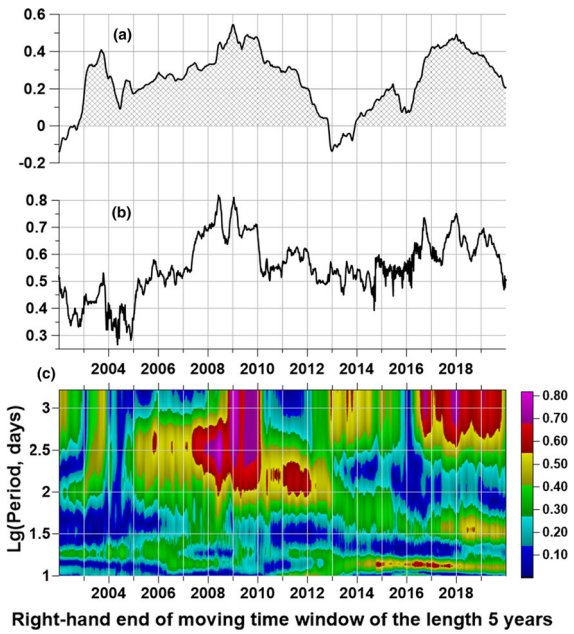

Figure 6
a A graph of the correlation coefficient between primary coherences calculated in a window with a length of 330 values (5 years); **b** a graph of the maximum coherence modulus between the primary coherences calculated in the same time window; **c** the time–frequency diagram of the estimation of the modulus of the coherence spectrum. All time marks correspond to the right-hand end of the moving time window

First of all, Fig. 6a shows that for most of the time windows, the correlation coefficient between the primary coherences in Japan and California is positive. This fact supports the hypothesis that the response of changes in the properties of seismic noise in these two remote regions has some synchronism. The absolute values of the correlation coefficient give a measure of the "strength" of the linear relationship between the two signals, but do not take into account the possible time shifts between them inside the time window. The spectral measure of coherence takes into account such shifts using the phase difference and, therefore, the modulus of the coherence spectrum must exceed the modulus of the correlation coefficient. Figure 6b shows a graph of the frequency maximum of the module of the coherence spectrum and we see that for each time window it significantly exceeds the module of the correlation coefficient.

The time–frequency diagram in Fig. 6c which is similar to Fig. 4a, presents a rather complicated pattern of the evolution of periods, which provide maxima of the "secondary" coherence module. If we compare the two time–frequency diagrams in Figs. 4a and 6c, then we can notice a common feature: time marks less than 2007 are characterized by small coherences for periods less than 100 days. Thus, we can assume that there is a certain general mechanism associated with the irregular rotation of the Earth, which controls both the synchronization of seismic noise properties (Fig. 4) and the synchronization of the reaction of changes in seismic noise properties to LOD variations in different regions of the Earth.

It is also possible to take into account the time shifts between primary coherences inside a long moving time window by calculating their correlation function. We denote by $C(t)$ and $J(t)$ the sequences of primary coherences for California and Japan, where t is the discrete time index. Within each time window, we calculate the correlation coefficients between $C(t)$ and $J(t + k)$, where the time shift k varies within range $-k_{\max} \le k \le k_{\max}$ and choose an

optimal time shift k^* for which the absolute value of the correlation coefficient is maximum.

Figure 7 shows the results of such an assessment. For a time window with a length of $L = 330$ values, we took the maximum time shifts $k_{\max} = 80$. When calculating the time shift in days, the obtained values k^* must be multiplied by 5, since the primary coherences are calculated in short time windows 182 days long with a shift of 5 days.

It can be seen from the graph in Fig. 7b that even with the introduction of mutual shifts between the primary coherences, the sign of the maximum absolute correlation coefficients remains mostly positive—the average value of correlations calculated for all time windows is 0.22, and their median is 0.42. This fact supports the hypothesis that the response of seismic noise properties in Japan and California to LOD changes is significantly synchronized.

9. Conclusion

A new method for analyzing the relationship between changes in the properties of seismic noise and irregular rotation of the Earth is proposed. The method is based on calculating in a moving time window the coherence between the principal components of the seismic noise properties and the time series of the day length LOD. The method is applied to the results of continuous synchronous monitoring of seismic noise over networks of broadband stations in Japan and California for 23 years, 1997–2019. The daily median values of two multifractal parameters, the generalized Hurst exponent and the singularity spectrum support width, as well as the minimum normalized entropy of the distribution of squared orthogonal wavelet coefficients, were selected as seismic noise properties. A significant relationship was found between the power of high-frequency (with periods of less than 6 days) LOD pulsations and the coherence between the properties of seismic noise in two regions which are essentially remote from each other as Japan and California. It turned out that the decrease in coherence for the time interval 1997–2007 is in clear antiphase with increasing variance of LOD. Further on, up to the time of the Tohoku mega-earthquake on March 11, 2011, a strong increase in coherence occurs, which confirms the earlier conclusion in Lyubushin (2017). It should be noted that after the Tohoku event, a rapid decrease in the LOD variance began, followed by reaching the stationary level. The degree of synchronization of the

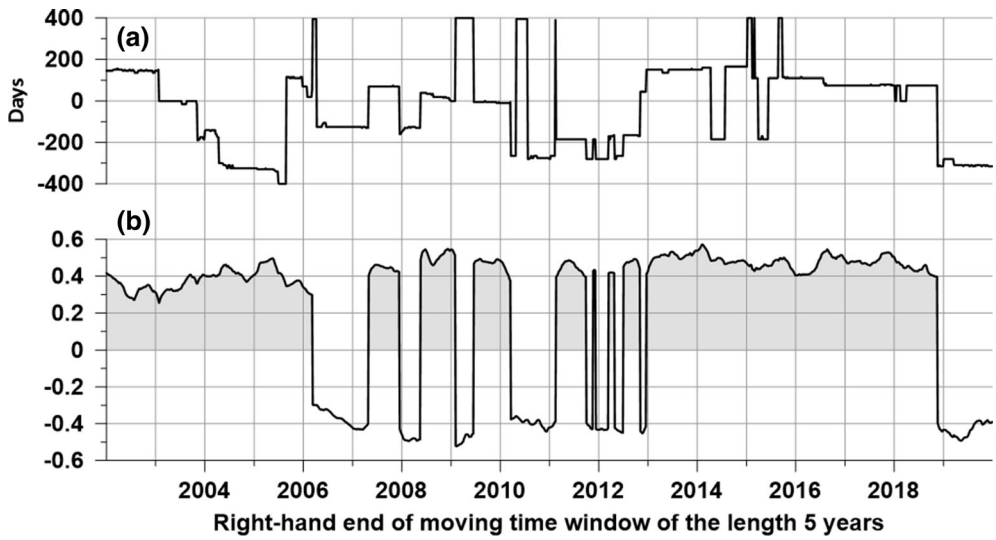

Figure 7
a Optimal time shifts between primary coherences for California and Japan, providing maximum values of the modulus of the correlation coefficient between themselves in time windows with a length of 330 values (5 years); **b** correlation coefficients having maximum absolute values after the corresponding mutual time shift

response of seismic noise properties in Japan and California to LOD changes was estimated by calculating the "secondary" coherences in a 5-year long time window between the "primary" coherences between the noise properties and LOD in short half-year windows.

Taken together, these facts confirm the hypothesis proposed in Lyubushin (2020) that the non-stationarity of high-frequency variations in the Earth's rotation regime affects the properties of seismic noise and their global correlations. Thus, the peculiarities of the irregular rotation of the Earth control both the synchronization of seismic noise properties and the synchronization of the reaction of changes in seismic noise properties to LOD variations in different regions of the Earth.

Acknowledgements

The research was supported by the Russian Foundation for Basic Research, Grant no. 18-05-00133, project "Estimation of fluctuations of seismic hazard on the basis of complex analysis of the Earth's ambient noise."

References

Ardhuin, F., Stutzmann, E., Schimmel, M., & Mangeney, A. (2011). Ocean wave sources of seismic noise. *Journal of Geophysical Research, 116*, C09004.

Aster, R., McNamara, D., & Bromirski, P. (2008). Multidecadal climate induced variability in microseisms. *Seismological Research Letters, 79*, 194–202.

Bendick, R., & Bilham, R. (2017). Do weak global stresses synchronize earthquakes? *Geophysical Research Letters, 2017*(44), 8320–8327. https://doi.org/10.1002/2017GL074934.

Berger, J., Davis, P., & Ekstrom, G. (2004). Ambient earth noise: A survey of the global seismographic network. *Journal of Geophysical Research, 2004*(109), B11307.

Costa, M., Goldberger, A. L., & Peng, C.-K. (2005). Multiscale entropy analysis of biological signals. *Physical Review E, 71*(2005), 021906.

Costa, M., Peng, C.-K., Goldberger, A. L., & Hausdorf, J. M. (2003). Multiscale entropy analysis of human gait dynamics. *Physica A Statistical Mechanics and its Applications, 330*(2003), 53–60.

Currenti, G., del Negro, C., Lapenna, V., & Telesca, L. (2005). Multifractality in local geomagnetic field at Etna volcano, Sicily (southern Italy). *Natural Hazards and Earth System Sciences, 5*, 555–559.

Dutta, S., Ghosh, D., & Chatterjee, S. (2013). Multifractal detrended fluctuation analysis of human gait diseases. *Frontiers in Physiology, 4*, 2013. https://doi.org/10.3389/fphys.2013.00274.

Feder, J. (1988). *Fractals* (p. 284). New York: Plenum Press.

Friedrich, A., Krüger, F., & Klinge, K. (1998). Ocean-generated microseismic noise located with the Gräfenberg array. *Journal of Seismology, 2*(1), 47–64.

Fukao, Y. K., Nishida, K., & Kobayashi, N. (2010). Seafloor topography, ocean infragravity waves, and background Love and Rayleigh waves. *Journal of Geophysical Research, 115*, B04302.

Grevemeyer, I., Herber, R., & Essen, H.-H. (2000). Microseismological evidence for a changing wave climate in the northeast Atlantic Ocean. *Nature, 408*, 349–352.

Humeaua, A., Chapeau-Blondeau, F., Rousseau, D., Rousseau, P., Trzepizur, W., & Abraham, P. (2008). Multifractality, sample entropy, and wavelet analyses for age-related changes in the peripheral cardiovascular system: Preliminary results. *Medical Physics American Association of Physicists in Medicine, 35*(2), 717–727.

Ivanov, P. C., Amaral, L. A. N., Goldberger, A. L., Havlin, S., Rosenblum, M. B., Struzik, Z., et al. (1999). Multifractality in healthy heartbeat dynamics. *Nature, 399*, 461–465.

Jolliffe, I. T. (1986). *Principal component analysis* (p. 487). Berlin: Springer. https://doi.org/10.1007/b98835.

Kantelhardt, J. W., Zschiegner, S. A., Konscienly-Bunde, E., Havlin, S., Bunde, A., & Stanley, H. E. (2002). Multifractal detrended fluctuation analysis of nonstationary time series. *Physica A Statistical Mechanics and its Applications, 316*(1–4), 87–114.

Kobayashi, N., & Nishida, K. (1998). Continuous excitation of planetary free oscillations by atmospheric disturbances. *Nature, 395*, 357–360.

Koper, K. D., & de Foy, B. (2008). Seasonal anisotropy in short-period seismic noise recorded in South Asia. *Bulletin of the Seismological Society of America, 98*, 3033–3045.

Koper, K. D., Seats, K., & Benz, H. (2010). On the composition of Earth's short-period seismic noise field. *Bulletin of the Seismological Society of America, 100*(2), 606–617.

Levin, B. W., Sasorova, E. V., Steblov, G. M., Domanski, A. V., Prytkov, A. S., & Tsyba, E. N. (2017). Variations of the Earth's rotation rate and cyclic processes in geodynamics. *Geodesy and Geodynamics, 2017*(8), 206–212. https://doi.org/10.1016/j.geog.2017.03.007.

Lyubushin, A. A. (2008) Multifractal properties of low-frequency microseismic noise in Japan, 1997–2008. In *Book of abstracts of seventh general assembly of the Asian Seismological Commission and Japan Seismological Society, 2008 Fall Meeting*, Tsukuba, Japan, 24–27 November 2008, p. 92.

Lyubushin, A. (2010). Multifractal parameters of low-frequency microseisms, in synchronization and triggering: From fracture to earthquake processes. In V. de Rubeis (Ed.), *GeoPlanet: Earth and planetary sciences 1, Chapter 15* (pp. 253–272). Berlin: Springer. https://doi.org/10.1007/978-3-642-12300-9_15.

Lyubushin, A. (2012). Prognostic properties of low-frequency seismic noise. *Natural Sciences, 4*(8A), 659–666. https://doi.org/10.4236/ns.2012.428087.

Lyubushin, A. (2013). How soon would the next mega-earthquake occur in Japan. *Natural Sciences, 5*(8), 1–7. https://doi.org/10.4236/ns.2013.58A1001.

Lyubushin, A. A. (2014a). Dynamic estimate of seismic danger based on multifractal properties of low-frequency seismic noise. *Natural Hazards, 70*(1), 471–483. https://doi.org/10.1007/s11069-013-0823-7.

Lyubushin, A. A. (2014b). Analysis of coherence in global seismic noise for 1997–2012. *Izvestiya, Physics of the Solid Earth, 50*(3), 325–333. https://doi.org/10.1134/S1069351314030069.

Lyubushin, A. A. (2015). Wavelet-based coherence measures of global seismic noise properties. *Journal of Seismology, 19*(2), 329–340. https://doi.org/10.1007/s10950-014-9468-6.

Lyubushin, A. A. (2017). Long-range coherence between seismic noise properties in Japan and California before and after Tohoku mega-earthquake. *Acta Geodaetica et Geophysica, 52*, 467–478. https://doi.org/10.1007/s40328-016-0181-5.

Lyubushin, A. (2018). Global coherence of GPS-measured high-frequency surface tremor motions. *GPS Solutions, 22*, 116. https://doi.org/10.1007/s10291-018-0781-3.

Lyubushin, A. (2018a). Synchronization of geophysical fields fluctuations. In T. Chelidze, L. Telesca, & F. Vallianatos (Eds.), *Complexity of seismic time series: Measurement and applications, Chapter 6* (pp. 161–197). Amsterdam: Elsevier. https://doi.org/10.1016/B978-0-12-813138-1.00006-7.

Lyubushin, A. A. (2018b). Cyclic properties of seismic noise and the problem of predictability of the strongest earthquakes in Japanese Islands. *Izvestiya, Atmospheric and Oceanic Physics, 54*(10), 1460–1469. https://doi.org/10.1134/S0001433818100067.

Lyubushin, A. (2019). Field of coherence of GPS-measured earth tremors. *GPS Solutions, 23*, 120. https://doi.org/10.1007/s10291-019-0909-0.

Lyubushin, A. A. (2020). Trends of global seismic noise properties in connection to irregularity of earth's rotation. *Pure and Applied Geophysics, 177*(2), 621–636. https://doi.org/10.1007/s00024-019-02331-z.

Mallat, S. (1999). *A wavelet tour of signal processing* (2nd ed.). San Diego: Academic Press.

Marple, S. L., Jr. (1987). *Digital spectral analysis with applications*. Englewood Cliffs: Prentice-Hall Inc.

Nishida, K., Kawakatsu, H., Fukao, Y., & Obara, K. (2008). Background Love and Rayleigh waves simultaneously generated at the Pacific Ocean floors. *Geophysical Research Letters, 35*, L16307.

Nishida, K., Montagner, J., & Kawakatsu, H. (2009). Global surface wave tomography using seismic hum. *Science, 326*(5949), 112.

Pavlov, A. N., & Anishchenko, V. S. (2007). Multifractal analysis of complex signals. *Physics Uspekhi Fizicheskikh Nauk Russian Academy of Sciences, 50*(8), 819–834. https://doi.org/10.1070/PU2007v050n08ABEH006116.

Ramirez-Rojas, A., Munoz-Diosdado, A., Pavia-Miller, C. G., & Angulo-Brown, F. (2004). Spectral and multifractal study of electroseismic time series associated to the Mw=6.5 earthquake of 24 October 1993 in Mexico. *Natural Hazards and Earth System Sciences, 4*, 703–709.

Rhie, J., & Romanowicz, B. (2004). Excitation of Earth's continuous free oscillations by atmosphere-ocean-seafloor coupling. *Nature, 2004*(431), 552–554.

Rhie, J., & Romanowicz, B. (2006). A study of the relation between ocean storms and the Earth's hum. *Geochemistry, Geophysics, Geosystems, 7*, 10. https://doi.org/10.1029/2006GC001274.

Sarlis, N. V., Skordas, E. S., Mintzelas, A., & Papadopoulou, K. A. (2018). Micro-scale, mid-scale, and macro-scale in global seismicity identified by empirical mode decomposition and their multifractal characteristics. *Scientific Reports., 8*, 9206. https://doi.org/10.1038/s41598-018-27567-y.

Shanker, D., Kapur, N., & Singh, V. (2001). On the spatio temporal distribution of global seismicity and rotation of the Earth—a review. *Acta Geodaetica et Geophysica Hungarica, 36*, 175–187. https://doi.org/10.1556/AGeod.36.2001.2.5.

Stehly, L., Campillo, M., & Shapiro, N. M. (2006). A study of the seismic noise from its long-range correlation properties. *Journal of Geophysical Research, 111*, B10306.

Tanimoto, T. (2001). Continuous free oscillations: Atmosphere–solid earth coupling. *Annual Review of Earth and Planetary Sciences, 29*, 563–584.

Tanimoto, T. (2005). The oceanic excitation hypothesis for the continuous oscillations of the Earth. *Geophysical Journal International, 160*, 276–288.

Taqqu, M. S. (1988). Self-similar processes. *Encyclopedia of statistical sciences, vol 8* (pp. 352–357). New York: Wiley.

Telesca, L., & Lovallo, M. (2011). Analysis of the time dynamics in wind records by means of multifractal detrended fluctuation analysis and the Fisher–Shannon information plane. *Journal of Statistical Mechanics: Theory and Experiment*. https://doi.org/10.1088/1742-5468/2011/07/P07001.

Varotsos, P., Sarlis, N., & Skordas, E. (2003). Long range correlations in the signals that precede rupture: Further investigations. *Physical Review E, 67*(021109), 13. https://doi.org/10.1103/PhysRevE.67.021109.

Varotsos, P. A., Sarlis, N. V., & Skordas, E. S. (2011). *Natural time analysis: The new view of time. Precursory seismic electric signals, earthquakes and other complex time series* (p. 449). Berlin: Springer.

Varotsos, P., Sarlis, N., & Skordas, E. (2013b). Attempt to distinguish electric signals of a dichotomous nature. *Physical Review E, 68*(031106), 7. https://doi.org/10.1103/PhysRevE.68.031106.

Zotov, L., Bizouard, C., & Shum, C. K. (2016). A possible interrelation between Earth rotation and climatic variability at decadal time-scale. *Geodesy and Geodynamics, 7*(3), 216–222. https://doi.org/10.1016/j.geog.2016.05.005.

(Received March 30, 2020, revised May 22, 2020, accepted May 29, 2020)